Transactions **of the SMiRT 27**
Yokohama, Japan, March 3-8, 2024
Division III

A NONLINEAR HYDROELASTIC FINITE ELEMENT MODELING OF A FLUID -STRUCTURE INTERACTION IN THE LARGE SIZE WATER NUCLEAR REACTOR POOLS

Alexander S Liberson[1], Dan M. Ghiocel[2]

[1] Senior Consultant, GP Technologies, Inc., New York, USA (alex.liberson@ghiocel-tech.com)
[2] President, GP Technologies, Inc., New York, USA (dan.ghiocel@ghiocel-tech.com)

ABSTRACT

An accurate representation of sloshing waves under an arbitrary seismic excitation of partially filled large size tanks/pools is crucial for the study of hydrodynamic load on the structural elements. The investigated fluid motion exhibits strong nonlinearity, sensitive to the fluid-structure hydro dynamic interaction. In this paper the finite element modelling of sloshing waves is carried out based on the fully non-linear wave potential theory. The validity of the approach is verified against published linear and non-linear analytical and numerical solutions as well as experimental measurements. The effect of the vertical baffles oriented in a longitudinal and transverse directions is analysed. The impact of bafflers elasticity is strictly local, affecting primarily the force exerted across the surface of the baffle. It was found that the baffle resilience found in FSI modeling is higher in comparison with a rigid baffle. When the excitation frequency is close to the natural frequency of the tank, the dynamics of the fluid becomes violent due to resonance leading to higher amplitudes of the surface waves and hydrodynamic force acting on the baffle. To reduce the sloshing wave effect in tanks, the baffle is widely used as a passive control, which is to dissipate the energy of the sloshing motion by segmenting the flow field of the tank into a number of sub-flow fields. The fluid hydrodynamic element is currently in the final QA verification and validation tests for implementation in the specialized ACS SASSI software for performing accurate fluid-soil-structure interaction (FSSI) analysis for nuclear structures including large tanks/pools.

MATHEMATICAL FORMULATION

Governing Equations and Boundary Conditions

The 3D unsteady hydro elastic problem considered is based on the assumption of the incompressible irrotational fluid and inviscid flow. These assumptions successfully describe the water behavior under nonlinear surface waves, as proved in multiple publications, e.g. (Dommermuth et al. 1988, Gagarina et al. 2014). Applying the definition of a velocity potential, $\boldsymbol{u} = \boldsymbol{\nabla}\varphi$, requirements for mass and momentum conservation can be expressed as follows:

$$\varphi_{xx} + \varphi_{xx} + \varphi_{xx} = 0, \qquad \text{in } \Omega \tag{1}$$

$$\varphi_t + \frac{1}{2}(\varphi_x^2 + \varphi_y^2 + \varphi_z^2) + gz + \frac{p}{\rho} = 0, \qquad \text{in } \Omega \tag{2}$$

where $\boldsymbol{u}$ is the vector velocity field, Ω denotes the 3D physical domain, ρ - water density, p – is the fluid pressure, φ – velocity potential, g – gravitational constant, x, y, z – Cartesian coordinates, t – time. Low indices indicate partial derivatives by the relating coordinate.

On the side walls and the bottom (assuming walls are rigid) the potential satisfies kinematic compatibility conditions

$$\varphi_n = \boldsymbol{U} \cdot \boldsymbol{n} \tag{3}$$

where $\boldsymbol{U}$ – is the velocity of the wall, and **n** is the outward normal to the wall**.** On the free surface, S, $z = \eta(x, y, t)$ the dynamic and kinematic conditions in a space fixed system can be written as:

$$\varphi_t + \frac{1}{2}(\varphi_x^2 + \varphi_y^2) + g\eta - \frac{1}{2}(\varphi_z^2)_{|S}(1 + \eta_x^2 + \eta_y^2) = 0, \qquad \text{at S(t):} \quad z = \eta(x, y, t) \tag{4}$$

$$\eta_t + \varphi_x\eta_x + \varphi_y\eta_y - (\varphi_z)_{|S}(1 + \eta_x^2 + \eta_y^2) = 0 \qquad \text{at S(t):} \quad z = \eta(x, y, t) \tag{5}$$

Finite Element Discretization

Consider a structured mesh, where i, j, k are the integer coordinates of nodes, vector coordinate **x** = (x, y, z), and two multi indices: I = (i , j , k), J=(I, j). The nodal discrete potential values $\varphi_I = \varphi_{ijk}$ are time dependent, $\varphi_I = \varphi_I(t)$. For simplicity, we use 3D quadrilateral elements with the standard three-dimensional piecewise linear continuous basis functions in space for the "interior" potential φ(**x**). The six simplest local basis functions in a cubic element are $N_I(\xi_1, \xi_2, \xi_3) = 1 \pm \xi_1 \pm \xi_2 \pm \xi_3), |\xi_i| \leq 1,$ defined by 6 local node values. On a free surface the truncated shape functions are used, $N_{0J}(\xi_1, \xi_2) = 1 \pm \xi_1 \pm \xi_2$. Physical coordinates and local reference coordinates are related by a mapping with the same standard shape basis functions. The FE interpolations φ_h and η_h are presented accordingly (The rule of summation is used that implies summation over the product of terms with repeated index)

$$\varphi \approx \varphi_h = \varphi_I(t)N_I(\xi_1, \xi_2, \xi_3) \tag{6}$$

$$\eta \approx \eta_h = \eta_J(t)N_{0J}(\xi_1, \xi_2) \tag{7}$$

The FE Galerkin procedure, applied to the equations (1-6) yields the following system of ordinary differential equations.

$$G_{II'}\varphi_{I'}(t) + R_M\delta_{IM} = 0 \tag{8}$$

$$M_{JK}\frac{d\varphi_J}{dt} + \frac{1}{2}(A_{JJ'K} - B_{JJ'K})\varphi_J\varphi_{J'} + \mathrm{g}M_{JK}\eta_J = 0 \tag{9}$$

$$M_{JK}\frac{d\eta_J}{dt} + A_{JJ'K}\eta_J\,\varphi_{J'} - D_{JK}\varphi_J = 0 \tag{10}$$

with the following matrix coefficients and vectors defined as

$$G_{II'} = \int_{\Omega_h}(\boldsymbol{\nabla} N_I \cdot \boldsymbol{\nabla} N_{I'})d\Omega\,; \qquad R_M = \int_{\Omega_h}(\boldsymbol{U} \cdot \boldsymbol{n})N_M d\Omega\,; \tag{11}$$

$$M_{JK} = \int_{\Omega_h}(N_{0J} \cdot N_{0K})d\Omega\,; \qquad A_{JJ'K} = \int_{\Omega_h}(\boldsymbol{\nabla} N_{0J} \cdot \boldsymbol{\nabla} N_{0J'})N_{0K}d\Omega \tag{12}$$

$$D_{JK} = \int_{\Omega_h}\frac{\partial N_J}{\partial z}N_{0K}d\Omega\,; \qquad B_{JJ'K} = \int_{\Omega_h}\left(\frac{\partial N_J}{\partial z} \cdot \frac{\partial N_{J'}}{\partial z}\right)N_{0K}d\Omega \tag{13}$$

where Ω_h indicate computational domain, multi-index M is used for the nodes located on walls. Equations (8)-(10) create a compact numerical stencil using minimum points for discretization. Numerical approximation is of the 2nd order accuracy in space, and the 4th order accuracy in time. The Gauss-Seidel method was used to solve the combined system of linear equations (8) and the nonlinear ones (9), (10). The 2D discrete FE model similar to (8) – (13) was presented in Gagarina et al. 2014.

Semi analytical approach for the implementation of elastic boundaries

Fluid flow interacting with resilient structures induces forces, which modifies in return the fluid domain, i.e. velocities and the pressure fields at the fluid-structure interface. To solve an FSI problem, two different approaches can be used. The first one is the strong coupling approach, where a single solver is in charge of the resolution of the complete system of equations, (Liberson et al. 2017). The second one is the weak coupling, (Felippa et al. 2001), where two solvers deal respectively with the fluid and the structure equations, and exchange information at the interfaces to ensure continuity of the variables.

The elastic baffle is regarded as the thin plate vibrating according to the Kirchhoff - Love two - dimensional model

$$\rho_w W_{tt} + D\Delta\Delta W = \hat{p} \tag{14}$$

where W – wall normal deflection, ρ_w - baffle's mass per unit area, $D = \frac{Eh^3}{12(1-\mu^2)}$ - flexural plate stiffness, E – elastic modulus, h – plate thickness, μ - Poisson coefficient, Δ - 2D Laplace operator, $\hat{p}$- net pressure, which is essentially the difference between pressures applied to the front and back surfaces. The specified boundary conditions relate to the clamped plate: zero deflection and zero slope with respect to the vertical direction at the root section of the baffles, while other boundary edges are free from transverse shear forces and bending moments. Initial conditions are zero, $W|_{t=0} = W_t|_{t=0} = 0$

Introducing the complete set of eigenfunctions, $W_k(y,z)$, $\Delta\Delta W_k = \lambda_k^4 W, (k = 1,2,\dots)$, we can expand normal deflection as

$$W(t,y,z) = \sum_k T_k(t) W_k(y,z) \tag{15}$$

Since the set of eigenfunctions is orthogonal and normalized, we can determine equations for $T_k(t)$by plugging (15) into equation (14) following by formation of the inner product with each of the elements of the set W_k. The described procedure yields the set of isolated ordinary differential equation

$$T_{k,tt} + \omega_k^2 T_k = \frac{1}{\rho_w}\int_{\Omega_B} \hat{p}(\xi,y,z)\, W_k(y,z)\, dydz, \qquad \omega_k = \lambda_k^2\sqrt{\frac{D}{\rho_w}} \tag{16}$$

Solution of (16) can be introduced in the closed form

$$T_k(t) = T_{k0}\cos(\omega_k t) + \frac{1}{\omega_k} T_{kt,0}\sin(\omega_k t) + \frac{1}{\rho_w \omega_k}\int_0^t \int_{\Omega_B} \hat{p}(\xi,y,z)\, W_k(y,z)\sin\big(\omega_k(t-\xi)\big)\, dydzd\xi \tag{17}$$

where $T_{k0}, T_{kt,0}$ are initial conditions for the $T_k(t)$ and its derivative
To specify kinematic compatibility of the flow encountering an elastic wall we need to differentiate (17) with the following use of equation (15). Setting to zero initial conditions velocity of the vibrating plate can be presented as the following:

$$W_t(t,y,z) = \sum_k W_k(y,z) \frac{1}{\rho_w} \int_0^t \int_{\Omega_B} \hat{p}(\xi,y,z)\, W_k(y,z) \cos\big(\omega_k(t-\xi)\big)\, dydz\, d\xi \tag{18}$$

Finally, the generalization of a kinematic condition (3) in case of elastic walls interacting with fluid, reads

$$\frac{\partial F}{\partial n} = (\boldsymbol{U} \cdot \boldsymbol{n}) + W_t \tag{19}$$

It should be noted that the net pressure acting upon the plate located in a flow field cannot be predicted within Eulerian flow model. According to the D'Alembert's paradox drag force within inviscid flow model is equal to zero, which addresses the related issue to the Navie-Stokes model capable to predict flow separation along with the Karman vortexes street. To circumvent the problem, we are using an engineering approach predicting drag pressure for the flat plate normal to the flow (Pritchard, Mitchel 2016) based on empirical drag coefficient as a function of Reynolds number, $\hat{p} = C_D \rho U_{rel}^2/2$, where drag coefficient C_D is independent of Reynolds number for Re>1000, $C_D = 2.05$, U_{rel} – velocity of the oncoming flow relative to the moving baffler.

VERIFICATION AND VALIDATION EXAMPLES

For verifying and validating the new hydrodynamic element modelling, we compared its results with proven and reputable existing simulation results from (Housner 1957, Ibrahim 2005, Ganuga et al. 2014), and with experimental analysis (Ganuga et al. 2014).

Figure 1 verifies against (Housner 1957) the following hydrodynamics parameters of the pool 40x10x10 m^3 subjected to the unidirectional axial acceleration: fluid flow acceleration as a function of axial coordinate x, pressure distribution in a vertical direction y relating to the 4 sections x=const, and the overall force exerted against 4 sections x=const as a function of x. The acceleration distribution shows symmetry, while the pressure and the force – anti-symmetry, which are prescribed by the symmetry of boundary conditions. 3D results are consistent with the modeling according to Housner's methodology.

The forced lateral unidirectional harmonic excitation of a rectangular tank was studied by (Ibrahim 2005). Figures 2-4 present the response of a fluid motion predicted by the present 3D numerical model and the Ibrahim's model. Comparison made relate to the amplitudes of dynamic parameters, proportional to the $\sin(\Omega t)$, where Ω – is a frequency of excitation.

Figure 2 presents distributions of the free surface undimensioned elevations (surface waves height), where the 3D model predicts slightly higher peaks of the wave amplitude.

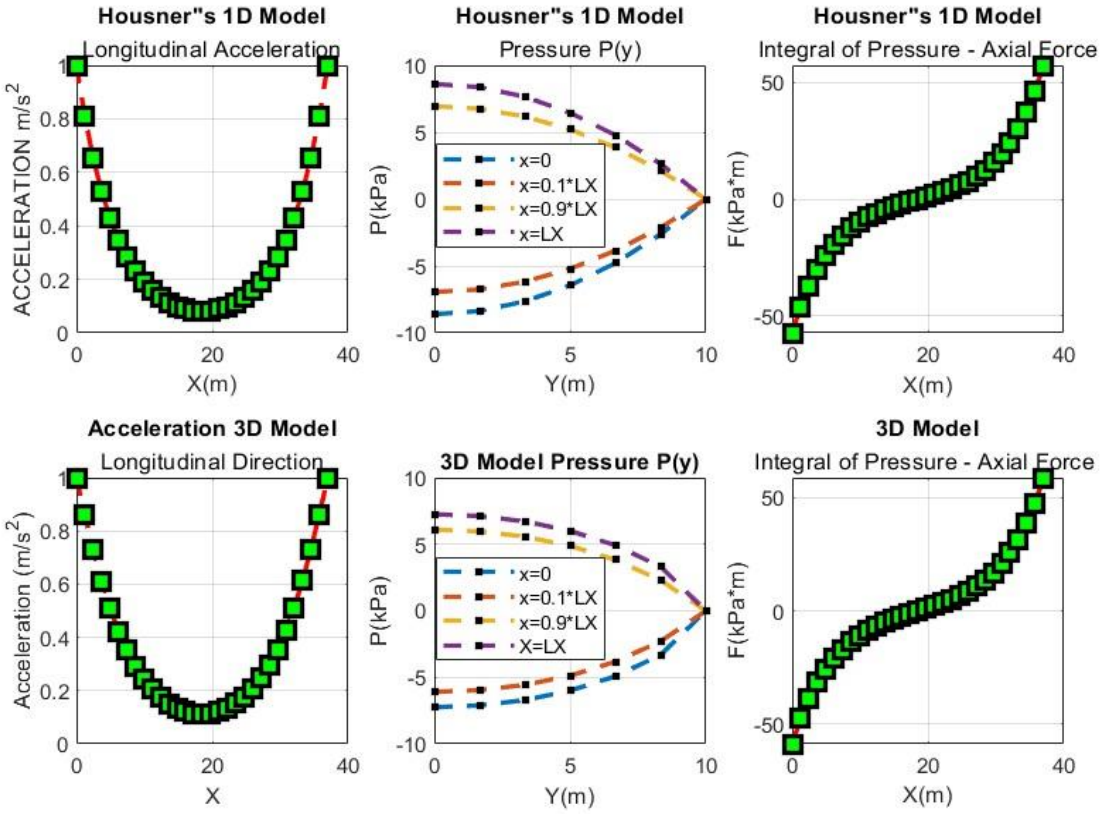

Figure 1. Comparative Analysis of a 3D Modeling with Housner's Model Results
The Upper Level Illustrates Housner's Results, the Lower Level – 3D

Figure 3 presents axial distributions of the perturbation pressure and the total pressure, where the perturbed pressure is calculating excluding linear pressure component due to the tank motion as a rigid body. Both distributions are anti symmetric with respect to the axial coordinate, which is prescribed by the symmetry of boundary conditions. Both models present almost identical results, slightly different at the terminal points relating to the wall

Figure 4 presents the absolute value of the total hydrodynamic force exerted by the fluid on the container wall as a function on unidimensional excitation frequency. Agreement in the proximity of the 1st resonance frequency is better than for the higher frequencies.

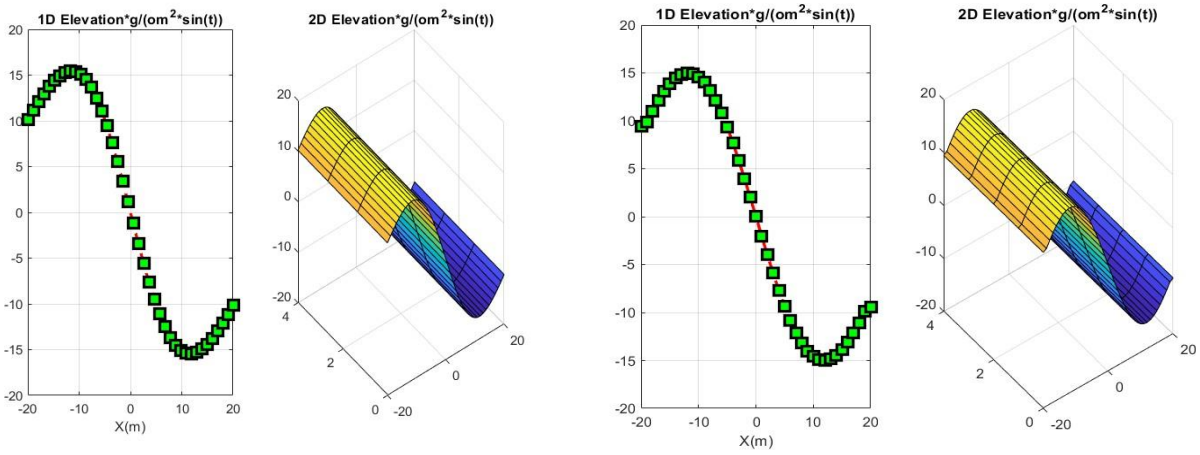

Figure 2. Free Surface Undimensioned Elevation According 3D (left) and Ibrahim's Models (right). (Ω - frequency of excitation, g – gravitational constant, t - time)

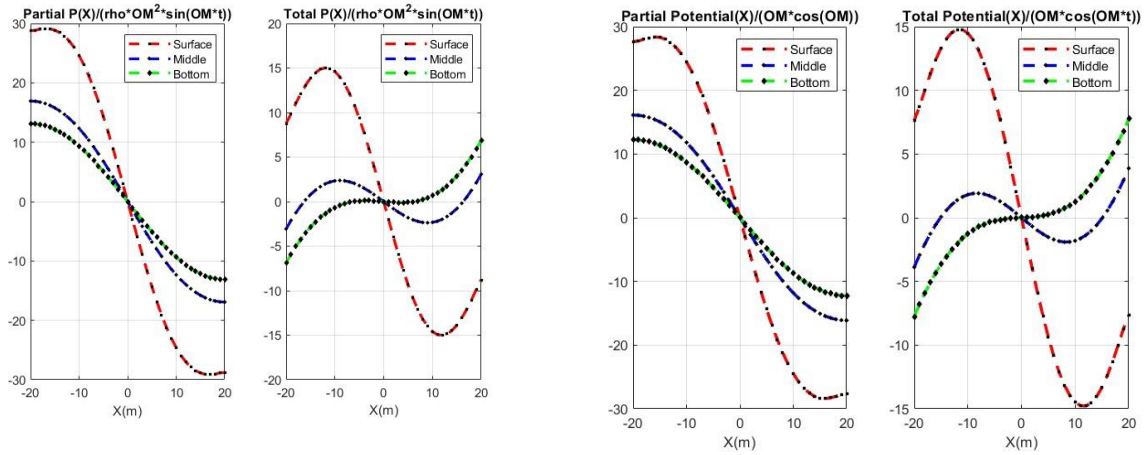

Figure 3. Perturbation and Total Pressure Distributions in Axial Direction According to 3D (left) and Ibrahims's Models (right) (rho – density of the fluid)

The time histories of the wave height at the tank wall obtained from the experiment and LS-DYNA modeling (Kozak et al. 2016) are compared with the 3D simulation results in Figure 5. The object is a rectangular tank of dimensions as 1.73 x 0.2 x 1.02 m^3. The prescribed harmonic motions (amplitude $\boldsymbol{\varepsilon_0}$, period *T*) were applied in longitudinal direction X. The forced oscillation period *T* was close to that of the fundamental mode of the fluid motion, *T*0, which affects dramatically the wave amplitude, making it comparable to the size of the tank.

Comparison of the FE prediction of the wave height maximum reached during 7 seconds with the LS-DYNA modeling and experimental data are presented in Figure 5, left (T=0.7sec, $\boldsymbol{\varepsilon_0 = 0.05m}$). The FE wave height prediction matches predictions made by LS-DYNA except some peak values which appear to be lower at LS-DYNA's distributions. The latter could be explained by the presence of a dissipation in viscous fluid model used by commercial software. On a right comparison of a nonlinear and linear FE models to experimental data presented (T=1.4 sec, $\boldsymbol{\varepsilon_0 = 0.05m}$). Nonlinearity affects primarily the peak values matching relating peaks measured experimentally.

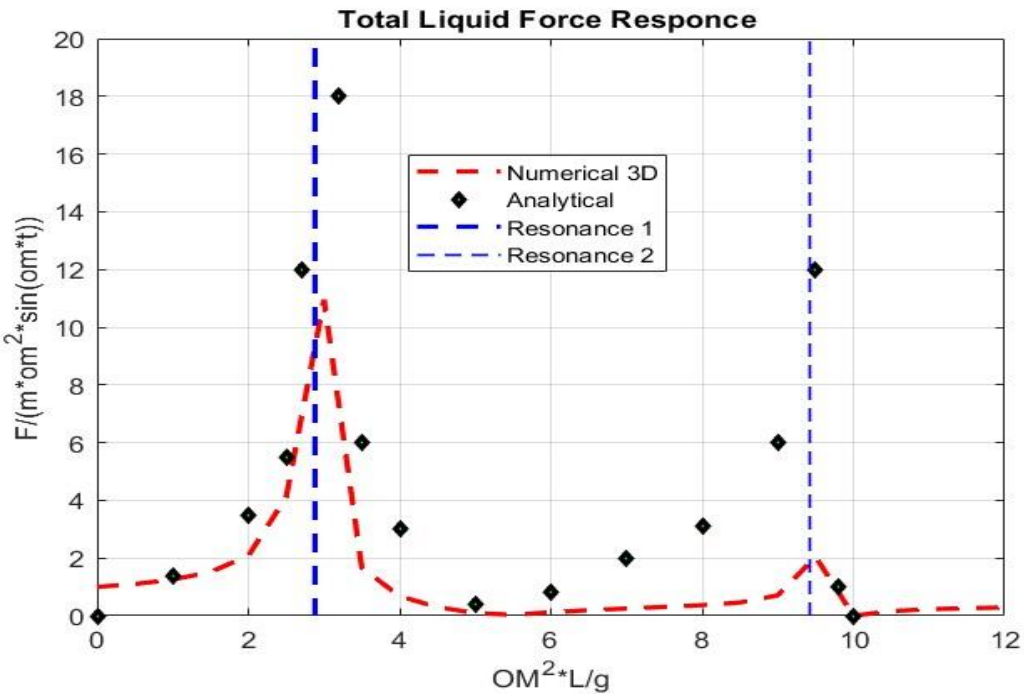

Figure 4. Total Hydrodynamic Force Amplitude Exerted on the Wall

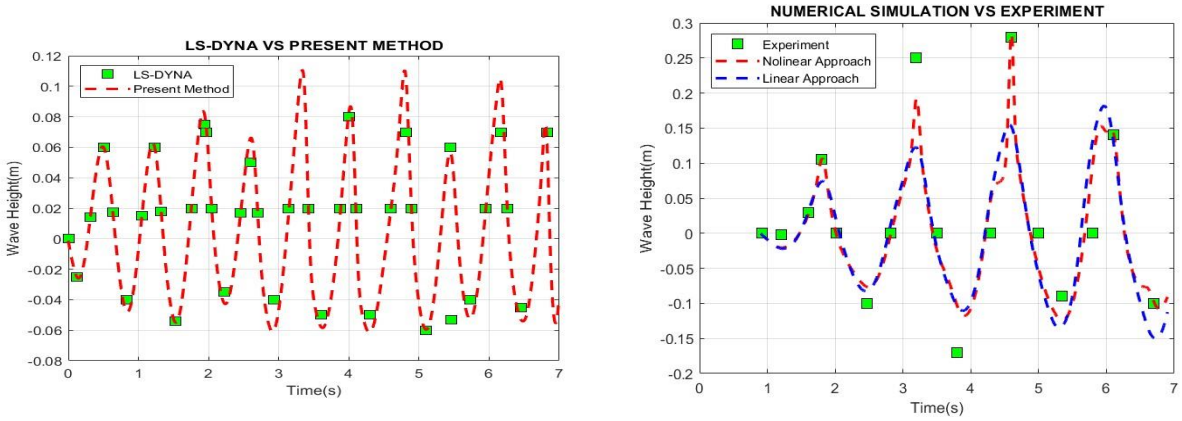

Figure 5. FE Prediction of the Wave Height Maximum vs LS-DYNA Modeling (Left) and Experimental Data (Right).

LARGE WATER POOL MODELING FOR SEISMIC ANALYSIS

A rectangular pool of the size 37 x 27 x 10 m^3 is studied under the impact of a 3D seismic waves characterized by three X, Y, Z components of acceleration and velocities as shown in Figure 6.

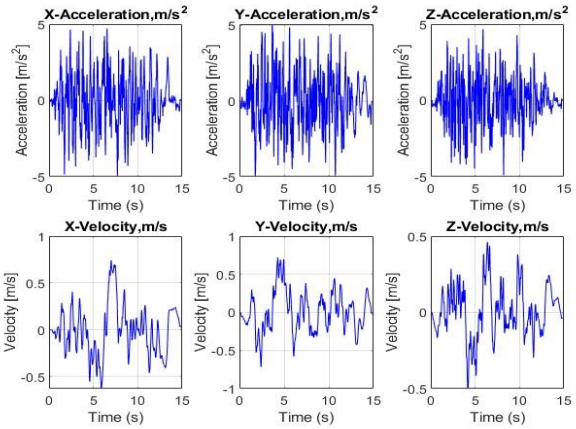

Figure 6. Time Dependent Acceleration and Velocity Components of Seismic Wave

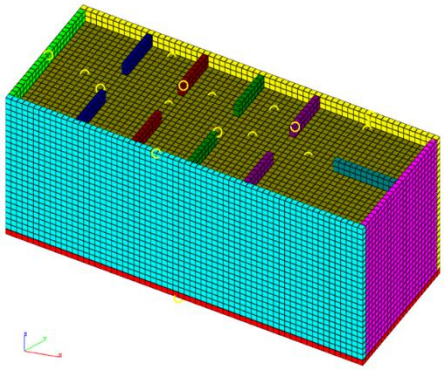

Fig.7 Water Tank With 7 Baffles

Analysis of a flow field distributions in a baffle free pool vs pool with 7 baffles (Figure 7) is presented in Figure 8. Baffles serve as a passive control capable to reduce energy of the sloshing motion as well as impact pressure exerted against wall as seen in Figure 8 by segmenting the flow field of the tank into a number of sub-flow fields bounded by internal walls (baffles).

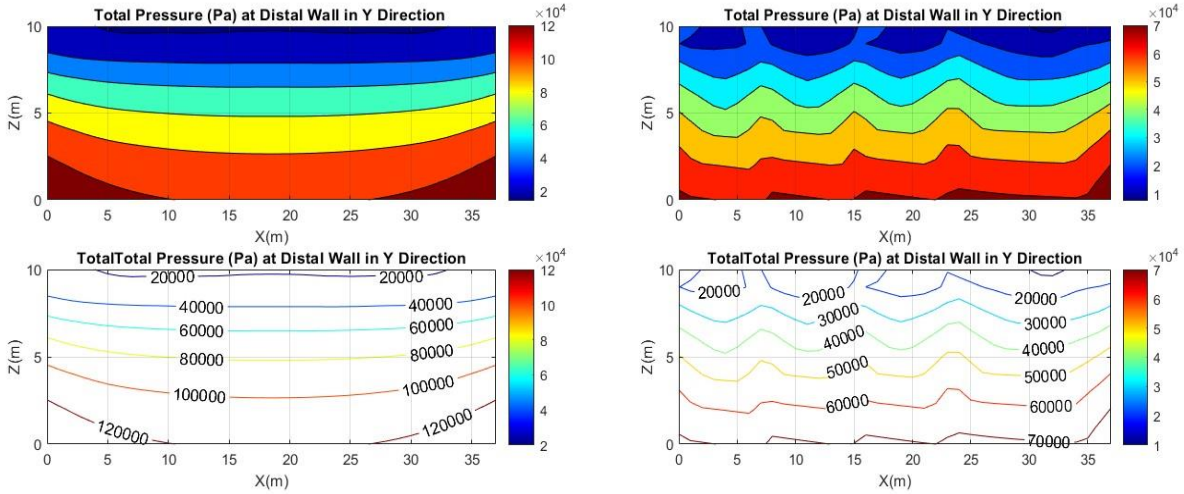

Figure 9. Pressure envelopes on a wall for the baffle free pool and a pool equipped with 7 baffles

Figure 10 illustrates effect of elasticity on the total force applied to the baffle.

The force acting against elastic wall exceeds its rigid wall counterpart, which correlates with the conclusions made in (Ganuga et al. 2014). Evaluation of the elastic baffle was processed using single eigen mode. The physical and geometric parameters of the baffle were used as the following: Young modulus E=200 GPa, Poisson coefficient μ=0.3, thickness h=15 mm, width b=1m, height h=8m.

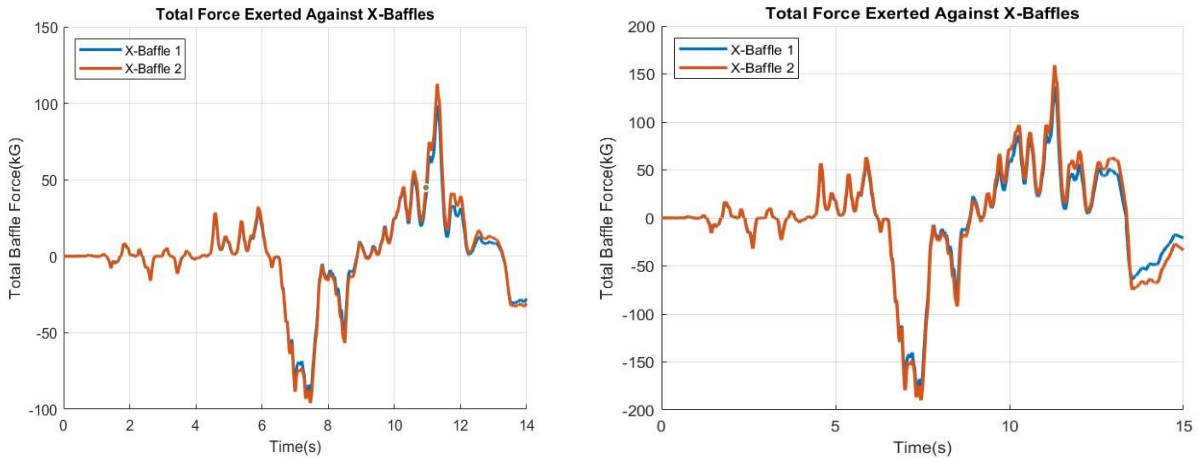

Figure 10. Total Force exerted against rigid (left) and elastic (right) baffles

CONCLUDING REMARKS

This paper focuses on the nonlinear sloshing wave problem in three dimensional baffled tanks based on a new implementation of a hydrodynamic finite element. The new hydrodynamic element is verified by comparing its results with the results from experiments and related literature. The sloshing characteristics are carried out, which are mainly concerned on the free surface elevation and hydrodynamic force exerted on the walls. The nonlinear hydrodynamic element is superior to the linear acoustic fluid elements as shown herein by the example against LS-DYNA and experiments.

It was found that the presence of baffles has a non-ignorable influence on the pressure distribution and the overall hydrodynamic field. It is concluded that the baffles can effectively serve as a passive control capable to reduce energy of the sloshing motion as well as impact pressure exerted against wall by segmenting the flow field of the tank into a number of sub-flow fields bounded by internal walls. Effect of wall's elasticity is essentially local, influencing mainly pressure distribution and the overall force applied to the internal wall surface.

REFERENCES

Dommermuth, D., Yue, D., Lin, W., Rapp, R., Chan, E. & Melville, W. 1988 *Deep-water plunging breakers: a comparison between potential theory and experiments.* J. Fluid Mech. 189, 423–442.

Felippa, C. A., Park K. C., Fahrat C. (2001*). Partitioned analysis of coupled mechanical systems.* ` *Computational methods in applied mechanical engineering*, 190, 3247–3270.

Gagarina, E., Ambati V.R., van der Vegt, J.J.W., Bokhove, O. (2014). *Variational Space-time (dis)continuous Galerkin Method For Nonlinear Free Surface Water Waves.* Journal of Computational Physics 275, 459-483

Ganuga R.S., Viswanathan H., Sonar S., Avasthi 2014. *Fluid-Structure Interaction Modelling of Internal Structures in a Sloshing Tank Subjected to Resonance*. International Journal of Fluid Mechanics. 41, 2, 145-168

GP Technologies (2023) *ACS SASSI NQA Version 4.3.6 - An Advanced Computational Software for 3D Dynamic Analysis Including Soil-Structure Interaction, Including Options A-AA and NON Advanced,* GP Technologies, Inc., User Manuals, Revision 8, New York, USA

Housner, G. W., 1957. *Dynamic Pressures on Accelerated Fluid Containers.* Bull. Seismological Society of. America 47(1), 15-35

Ibrahim R.A. 2005. *Liquid Sloshing Analysis. Theory and applications*. Cambridge University Press. 947p

Kozak A.I., Tehrani P.K., Abrahamson T.E., Krimotat, A.V. 2017. *Validation of the ALE Methodology by Comparison with the Experimental Data Obtained from a Sloshing Tank*. 14th International LS-DYNA Users Conference, 1-14

Liberson, A.S, Seyed Vahedein, Y., Borkholder D.A. (2017). *Variational Approach of Constructing Reduced Fluid-Structure Interaction Models in Bifurcated Networks*. Proceedings of the 2nd World Congress on Momentum, Heat and Mass Transfer (MHMT'17) Barcelona, Spain – April 6 – 8, Paper No. ENFHT

Pritchard P.J., Mitchell J.W. (2016). *Fox & McDonald's Introduction to Fluid Mechanics. Introduction to Fluid Mechanics*. *Science, 672 p.*